Desalination and Water Treatment
www.deswater.com
doi: 10.5004/dwt.2020.24902

175 (2020) 263–272
January

The catalytic activity of the coupled CdS-AgBr nanoparticles: a brief study on characterization and its photo-decolorization activity towards methylene blue

Seyyedeh Atefeh Mirsalari[a,b], Alireza Nezamzadeh-Ejhieh[a,b,c,*]

[a]*Department of Chemistry, Shahreza Branch, Islamic Azad University, P.O. Box: 311-86145, Shahreza, Isfahan, Iran, Tel. +98 31-53292515; Fax +98 31-53291018; email: atefemirsalari236@yahoo.com (S.A. Mirsalari), Tel. +98 31-53292500; email: arnezamzadeh@iaush.ac.ir (A. Nezamzadeh-Ejhieh)*
[b]*Young Researchers and Elite Club, Shahreza Branch, Islamic Azad University, Shahreza, Iran*
[c]*Razi Chemistry Research Center (RCRC), Shahreza Branch, Islamic Azad University, Isfahan, Iran*

Received 25 April 2019; Accepted 10 September 2019

ABSTRACT

As synthesized coupled CdS-AgBr nanoparticles (NPs) (CCAN) were characterized by X-ray diffraction, scanning electron microscopy, photoluminescence and ultraviolet-visible diffuse reflectance spectroscopy techniques. The surface charge of the individual CdS NPs, AgBr NPs and the resulted coupled CdS-AgBr system was estimated at 6.3, 4.6, and 5.6, respectively. Then, the photocatalytic activity of the individual and the coupled systems was tested towards decolorization of methylene blue (MB) in aqueous solution and about 39%, 60%, and 80% of MB molecules were respectively decolorized by CdS NPs, AgBr NPs, and CdS-AgBr CCAN during 30 min photocatalytic decolorization experiments. Change in a mole ratio of the involved semiconductors of the coupled system changed the photo decolorization activity and the best response was obtained for the catalyst with a mole ratio of 1:4 CdS:AgBr. Kinetic of the process was followed and the results showed that the Langmuir-Hinshelwood model can model the process and a relatively fast reaction with a rate constant about 3.49×10^{-2} min^{-1} was distinguished. Mineralization extent of MB aqueous solution during the decolorization experiments was followed by chemical oxygen demand (COD) technique and the results showed that the initial COD value of 1,280 mg O_2 L^{-1} was decreased to 640 and 480 mg O_2 L^{-1} after 30 and 60 min of decolorization of MB solution. The catalyst retained its initial activity during 4 successive reusing runs.

Keywords: CdS-AgBr nano-composite; Heterogeneous photocatalysis; Methylene blue; Langmuir-Hinshelwood

1. Introduction

Increased using of dye compounds in different industries such as textile, food, laser, pharmaceutical, solar cells, etc. have caused serious contamination of the environment in recent decades. Especially, effluents from textile industries have well known as very dangerous polluted systems because of their carcinogenic, allergic, mutagenic, and genotoxic contents [1–5]. So far, different physical, chemical, or biological processes (or in some cases a combination of the methods) have been used for removing different organic/inorganic pollutants or to eliminate solids (or in some cases nutrients) from water/wastewater samples [6–20]. In physical methods (such as coagulation, filtration, flocculation, precipitation, solvent extraction, ion exchange, etc.) the waste material is isolated or separated from the mainstream. These methods involve little or no degradation of the waste and commonly transfer the pollutant from one phase to another that need further purifications. Other disadvantages of these methods are high-energy requirements and production of

* Corresponding author.

toxic sludge or other waste products that require further disposal. The biological treatment method needs to especial care like pH and aeration to hold the microbes' activities because the main process is the use of microbes to feed on the organic waste [21,22].

There are some recalcitrant contaminants in wastewater that resist elimination by generally applied physical and/or chemical treatment processes. In such cases, chemical oxidation processes can be used to destroy these stable compounds through oxidation and reduction reactions. This chemical method has a common name of an advanced oxidation process (AOP). This method is based on the production of different reactive radicals such as hydroxyl, superoxide, and sulfate radicals, etc. as the powerful oxidants for non-selectively destroying of different organic materials and their degradation intermediates. However, the hydroxyl radical is known as the main radical that is responsible for the degradation of organic pollutants. This powerful radical can be generated in different AOP methods such as ozonation, O_3/H_2O_2, H_2O_2/UV, Fenton's process (Fe(II)–H_2O_2), heterogeneous photocatalysis, etc. [21–23]. In spite of the cost-effective property of the common homogeneous Fenton systems as a source of hydroxyl radicals, some major drawbacks limited its industrial applications. These drawbacks can be classified to (a) the suitable pH range of the reaction, (b) the recovery of the precipitated catalyst at the end of the process, and (c) interfering effects of some ion-complexing agents such as phosphate anions that can deactivate the catalyst. In addition, further treatment of the resulting sludge (that contains organic substances as well as heavy metals) may increase the overall cost of the process [22].

Thus, the heterogeneous photocatalysis based on the semiconducting materials has been widely used as the most effective, green, cost-effective environmentally friendly AOP technique. In this technique, when the used semiconductor is irradiated by a photon with adequate energy equal or greater than the bandgap energy of the semiconductor, the photogenerated electrons and holes (e^-/h^+ pairs) can generate in its conduction (C_b) and valence (V_b) bands, respectively. These e^-/h^+ pairs can react with dissolved oxygen and water molecules (or hydroxyl anions) and produce $^{\bullet}O_2^-$ and $^{\bullet}OH$, respectively. All generated reactive species (e^-/h^+ pairs and the radicals) can attack the organic/inorganic pollutants present in media and break them into smaller fragments. Especially, hydroxyl and superoxide radicals can act as non-selective oxidants for destroying different organic pollutants. This non-selective property is an important advantage of the semiconducting based photodegradation processes because these radicals can destroy different pollutants in water and finally mineralize the degradation products to water and carbon dioxide molecules. This is very important because some degradation intermediates are more toxic than the parent pollutant molecules and if these radicals act selectively, the toxicity of some systems may be increased during the photodegradation process [24–29].

Unfortunately, e^-/h^+ recombination in such systems can decrease their efficiency and consume the energy as heat and thus increase the cost of the method. So far, doping of some metals into the semiconductors, coupling of two or more semiconductors, supporting of them onto a suitable support such as zeolites etc. have been used by researchers to diminish the rate of e^-/h^+ recombination and increase the efficiency of the semiconducting based photodegradation processes [30–38].

In this work, AgBr nanoparticles (NPs) (as a *p*-type semiconductor) and CdS NPs (as an *n*-type semiconductor) were coupled to increase their photocatalytic activities in photo decolorization of methylene blue (MB). Although MB (or methylthioninium chloride) is well known as a dye, but it also has known a medication to treat methemoglobinemia that treats methemoglobin levels greater than 30% or in which there are symptoms despite oxygen therapy. In addition, its use in cyanide poisoning and urinary tract infections has no longer recommended. Generally, MB with wider applications including textile, leather, pulp, and paper, temporary hair colorant, dyeing cotton, wools, coating for paper stock and as analytical reagent can easily adsorb onto the surface of solids that favors conditions for its better photodegradation. Cationic MB thiazine dye has common side effects including confusion, headache, shortness of breath, vomiting, and high blood pressure. Its other side effects are serotonin syndrome, red blood cell breakdown, and allergic reactions. Its common use changes the blue color of the urine, sweat, and stool to green. It is using during pregnancy can harm the baby, not using it in methemoglobinemia is likely more dangerous. It acts by converting the Fe(III) ions in hemoglobin to Fe(II) ions. Due to these side effects removing it from aquatic systems has got great importance and commonly used as the model pollutant in the photodegradation process. It is a visible light active compound. It undergoes decolorization upon reduction and its two electrons reduction process gives the colorless (λ_{max} = 256 nm) leuco-methylene blue (LMB), but and one-electron reduction process changes it to pale yellow (λ_{max} = 420 nm) anion-radical MB^-, which rapidly disproportionates to MB and LMB [39–43].

Different characterization techniques were applied to characterize the as-synthesized coupled system. In the photo-decolorization of MB, after performing some preliminary experiments, the kinetic of the process was followed.

2. Experimental

2.1. Chemicals and synthesis

All chemicals used (cadmium nitrate, silver nitrate, $(NH_4)_2S$, NaBr) were of analytical reagent grade and purchased from Merck-Aldrich Co. (India) or Fluka Co. and used without further purification. Commercial MB dye (molecular formula: $C_{16}H_{18}Cl\ N_3S$) was purchased from local chemical stores. All solutions/suspensions were prepared in distilled water.

For synthesis of CdS NPs, 100 mL 0.085 mol L^{-1} of $Cd(NO_3)_2$ solution was added dropwise into a 100 mL 0.1 mol L^{-1} of $(NH_4)_2S$ solution at 1,200 rpm stirring and continued for 5 h. The resulting dark yellow CdS NPs were obtained at the end of the process [44].

For the synthesis of AgBr NPs, 50 mL 0.1 mol L^{-1} of the $AgNO_3$ solution was added into a 20 ml portion of 0.25 mol L^{-1} of NaBr solution and then was kept at 60°C for 1 h. The resulted golden yellow precipitate was separated by centrifugation at >13,000 rpm. Then it was washed with water and ethanol repeatedly, and dried in vacuum [45].

For the preparation of the coupled AgBr-CdS system, an adequate amount of each semiconductor (corresponding to the desired mole ratio of the semiconductor in the composite) was added in an agate mortar and hand-mixed thoroughly for 10 min.

2.2. Characterization methods

The instruments used for the characterization of the samples in this work are listed below. A X-ray diffraction (XRD) (model: X'PertPro, Netherland, filter: Ni, Source: Cu-K_α at 1.5406 Å, *V*: 40 kV, *i*: 30 mA), an UV–Vis diffuse reflectance spectrophotometer (JASCO V-670, $BaSO_4$ as reference, Japan), a scanning electron microscopy (SEM), (model: MIRA3LMU, TESCAN Co., Czech Republic), a photoluminescence (PL) spectrophotometer (PerkinElmer, LS 45, UK), an ultraviolet-visible (UV-Vis) double beam spectrophotometer (UV/Vis 2100S, JASCO (Japan), power source: AC 220 V/50 Hz, quartz cells), a centrifuge instrument (Sigma, rpm: 13,000, g: 15493), a high-performance liquid chromatography instrument (Agilent 1200, Column: Zorbax@5 μm Eclipse-XDB-C_{18} 80 Å), and a Jenway *p*-ion meter device (model 3505).

2.3. Photo-decolorization experiments

A 10 mL 2 ppm MB solution at pH 7.8 containing 1 g L^{-1} of the catalyst (as single semiconductor or the coupled system) was irradiated by a moderate pressure W-lamp (35 W, Philips, type G-line with maximum emission at 435.8 nm) in a quartz cell. A portion of the suspension was withdrawn at definite times and centrifuged at 13,000 rpm. The absorbance of the cleaned supernatant (*A* corresponds to concentration *C*) was read at 664 nm. By using the recorded absorbencies of the MB solutions before (A_0 correspond to C_0) and after the irradiation process, the C/C_0 values were determined as a measure of the decolorized MB molecules. Also, the decolorization extent of MB molecules was estimated by the following equation.

$$\text{Decolorized MB}\ (\%) = \left[\frac{(C_0 - C)}{C_0}\right] \times 100 \quad (1)$$

3. Results and discussion

3.1. Characterization

3.1.1. XRD patterns

To determine the crystallite phase of the prepared coupled AgBr-CdS catalyst, it was subjected to XRD analysis which of recorded XRD pattern is shown in Fig. 1a. Typical diffraction peaks have been reported for the cubic phase of AgBr that positioned at 2θ values of 26.7° (111), 30.6° (200), 44.3° (220), 52.7°, 55.1° (222), 64.5° (400), and 73.3° (420) according to JCPDS File No. 06–0438. The values in parenthesis are corresponding hkl crystal planes (Miller indices) [46].

Based on literature [47], the hexagonal (wurtzite) phase of CdS crystals includes the main XRD peaks at 2θ positions of 24.96° (100), 26.63° (002), 28.31° (101), 43.71° (110), 47.86° (103) and 51.85° (112) and two weaker peaks of 66.61° (203) and 69.09° (210) (JCPDS No. 41–1049). Also, it is cubic (Zinc blend, β-CdS) phase includes the main peaks at 2θ values of 26.7° (111), 44° (220) and 52° (311) (JCPDS 00-042-1411) [48]. As shown in Fig. 1a, the XRD pattern of as-synthesized CdS agrees with that of the cubic CdS phase. The important peaks of AgBr and CdS crystals are assigned in Fig. 1a. As obvious, the coupled system includes the cubic AgBr and CdS crystallite phases.

To estimate the crystallite phase of the coupled system, the following Scherrer equation was used at which λ is the applied X-ray wavelength (CuKα, 1.5406 Å), θ the Bragg angle, *K* the Scherrer constant (0.9) and β is the full width at half maximum (FWHM) [49,50]. All information used for this calculation are summarized in Table S1. The average crystallite size of the coupled AgBr-CdS system was estimated at 29 ± 5 nm.

$$d = \frac{(K\lambda)}{(\beta\ cos\theta)} \quad (2)$$

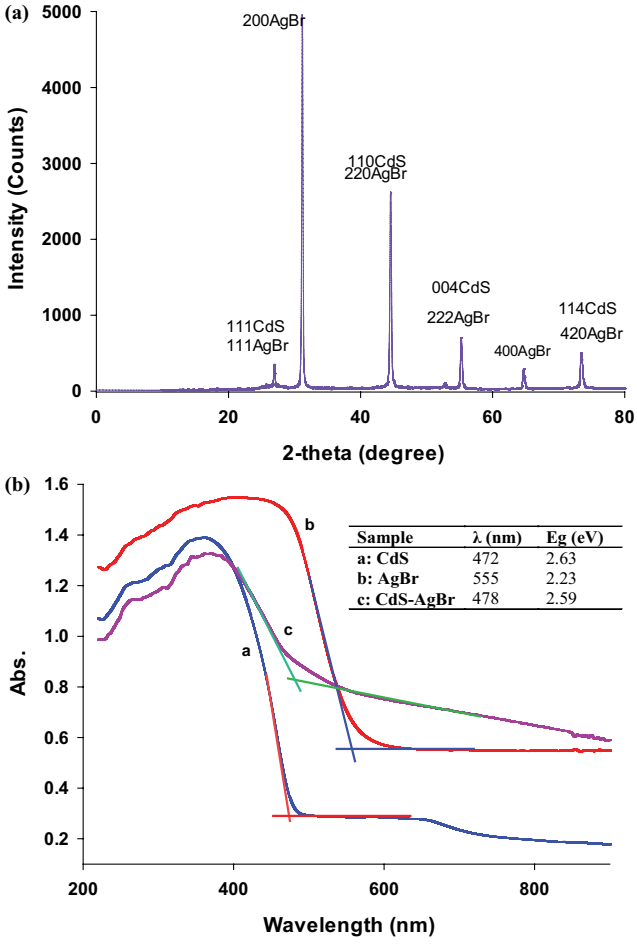

Fig. 1. (a) XRD pattern of the coupled AgBr-CdS catalyst with a mole ratio of 4:1 and (b) typical absorption spectra of the as-synthesized AgBr and CdS NPs and their coupled AgBr-CdS catalyst obtained in UV-Vis spectroscopy.

3.1.2. Estimation of the bandgap energy of the samples

In UV-Vis diffuse reflectance spectroscopy, the interactions of a typical semiconductor photocatalyst with photon energies can be investigated. In the fundamental absorption, an electronic excitation can occur from the V_b (valence band) to the C_b (conduction band). This electronic transition can be used for the determination of the nature and value of the optical bandgap (E_g) of the subjected semiconductor [51]. Typical absorption spectra of the as-synthesized single CdS and AgBr and their coupled CdS-AgBr are shown in Fig. 1b. The corresponding absorption edges were estimated at 472, 555, and 478 nm by extrapolation of the curves. These values were used for the calculation of their bandgap energies by using the following equation [52].

$$E_{bg}\left(\text{eV}\right)=\frac{1,240}{\lambda\left(\text{nm}\right)} \tag{3}$$

where λ is the wavelength of the absorption edge. Accordingly, the bandgap values of 2.63, 2.23, and 2.59 eV were respectively obtained for CdS, AgBr NPs and the corresponding coupled AgBr-CdS system. As shown, the coupled AgBr-CdS system showed a blue shift in the bandgap with respect to AgBr NPs while it showed a small redshift with respect to CdS NPs. This confirms that the optical properties of AgBr was significantly enhanced when it was coupled with CdS NPs.

3.1.3. PL spectra

PL spectroscopy is a non-destructive probe to study the electronic structure of materials. In a photo-excited material, the excess energy of the material, that saved by absorption of a photon energy, can be dissipated by the material through the emission of light, or PL. All electronic transitions must occur within the permissible states of the materials. Typically in semiconducting materials, these permissible energy states called conduction (C_b) and valence (V_b) bands. Hence, the released energy or the energy of the emitted photon corresponds to the bandgap energy of the subjected semiconductor. But, the quantity or the intensity of the emitted photons correspond to the relative recombination of the photogenerated e^-/h^+ pairs, as the most important drawback of a typical photodegradation process. Hence, a high intense PL spectrum shows a fast and high e^-/h^+ recombination process and the lowest photodegradation efficiency [53].

To follow the goodness of the coupling of CdS and AgBr NPs for reducing the e^-/h^+ recombination process, PL spectra of CdS and AgBr NPs and their coupled system were recorded which of results are shown in Fig. 2a. As shown, a drastic decrease in PL intensity was observed when the individual semiconductors were coupled. This confirms a significant decrease in the rate of e^-/h^+ recombination that elongated e^-/h^+ pairs lifetimes. Hence, the photogenerated e^-/h^+ pairs have enough time to reach the surface of the coupled catalyst and participate in the redox process. This significantly enhances the photodegradation of MB molecules.

Fig. 2b shows PL spectra of the coupled systems when the moles of the involved semiconductors were changed. As shown, PL intensity is a mole ratio-dependent process for

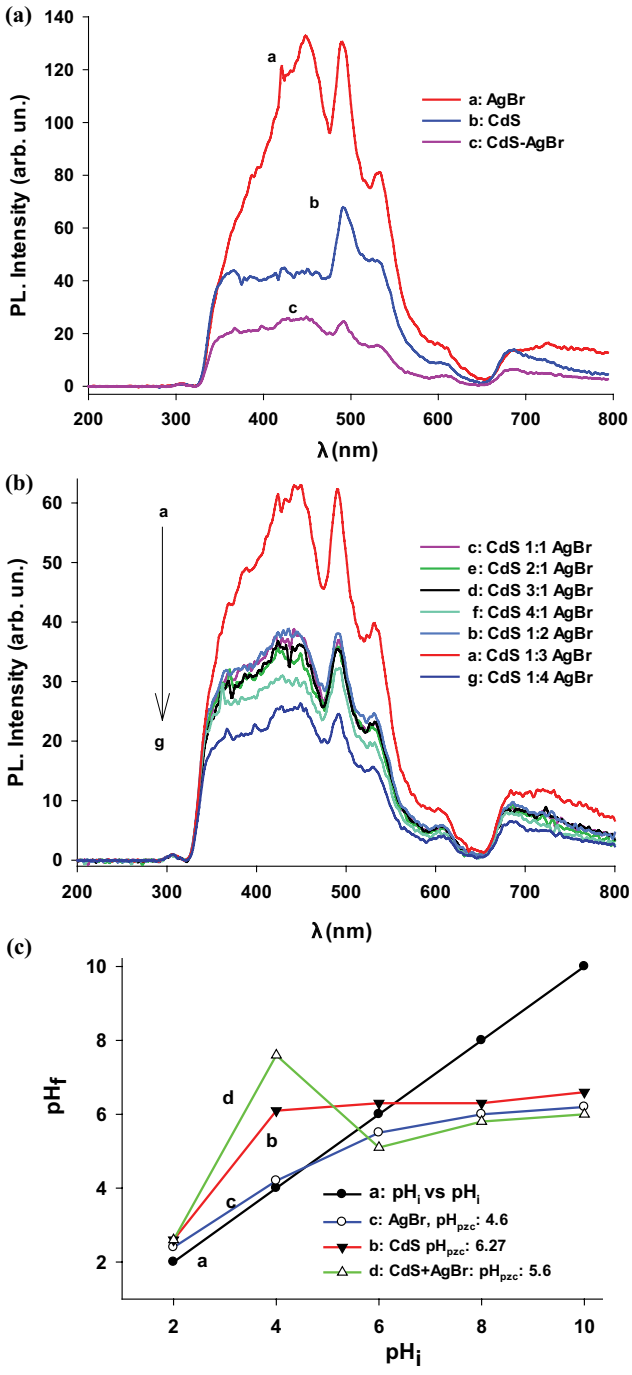

Fig. 2. (a) Photoluminescence spectra (PL) of the CdS, AgBr and CdS-AgBr photocatalysts, (b) PL spectra of the CdS, AgBr and CdS-AgBr photocatalysts in different mole ratio (conditions in both cases: 100 mg L^{-1} in acetone, λ-excitation: 300 nm, 10 min ultra-sonic), and (c) typical plot for calculation of pH_{pzc} of individual AgBr and CdS and their composite.

the investigated catalysts. In general, change in the mole ratio of the involved semiconductors caused to both e^-/h^+ production and decrease in e^-/h^+ recombination processes. Hence, PL intensity changed by changing the mole ratio of CdS and AgBr in the coupled system. As shown the lowest PL intensity

was observed for the coupled system that mole of AgBr ingredient is 4 times greater than that of the other ingredient. This catalyst showed the maximum photocatalytic activity in the photodegradation of MB aqueous solution which of results will discuss in the photodegradation section.

3.1.4. Surface charge and morphology of the samples

To investigate the surface charge of the catalysts, initial pH (pH_i) of a set of suspensions (0.15 g of each catalyst in 25 mL 0.1 M NaCl, for fixing the ionic strength) was recorded and after 24 h shaking (150 rpm), the final pH (pH_f) was recorded. The plot of the pH_i vs. pH_f was constructed and the crossing of the curve with the diagonal bisector line (pH_i vs. pH_i) gave the pH_{PZC} values (the point of zero charges) for the investigated catalysts [54]. The typical plot is shown in Fig. 2c at which the values of 4.6, 6.3, and 5.6 were determined as pH_{PZC} for AgBr, CdS, and the AgBr-CdS systems, respectively.

In general, before the pH_{PZC} value, the surface of the catalysts has a basic property (or a negative charge) and hence adsorb the protons in the contacted solution. This results in a net positive charge for the catalyst surface and increases the pH of the contacted solution. For example, the initial pH 4 was changed to 4.2, 6.1, and 7.6 for AgBr, CdS and the coupled samples, respectively. At pH > pH_{PZC}, due to acidic property of the catalyst surface (or its positive charge), its surface adsorbs the hydroxyl radicals from the adjacent aqueous solution and hence gets a net negative charge. At this time, the pH of the adjacent solution tends to decrease. For example, the initial pH 8 was changed to 6.0, 6.3, and 5.8 for AgBr, CdS and the coupled samples, respectively. At pH_{PZC} point, the surface charge of the catalyst is equal to that of the adjacent solution and hence it has a net-zero charge. On the other hand, at this point, the basic property of the catalyst surface begins to change to the acidic property [55].

The surface charge of the catalyst/adsorbent surface plays an important role in the adsorption phenomena and the catalytic activity of the catalyst. On the other hand, in cases at which there are repulsive forces between the catalyst surface and the ionic forms of the subjected analyte in solution, it can even limit the advantages of the high surface area of the catalyst/adsorbent and can reduce the efficiency of the process. It is worth mentioning that, a typical catalytic process occurs on the surface of the catalyst and hence knowing about the surface charge of the catalyst is very important to optimize the conditions for reaching the best efficiency [55].

The SEM images of the coupled system were recorded and some images are shown in Fig. 3. As shown, some particles were aggregated. Generally, most particles have uniform morphology and the smallest particles were dispersed around the aggregated particles. To have an estimation about the particle size of the coupled semiconductors, image-j software was applied on the image (c) and the results are summarized in Fig. 3d. The results confirm that most of the particles have nano-dimension below 80 nm.

3.2. Photocatalytic decolorization results

3.2.1. Boosted effect of the semiconductors

Change in the UV-Vis absorption spectra during the surface adsorption, direct photolysis and the photocatalytic decolorization processes on the removal of MB molecules from its aqueous solution was recorded. The obtained results are shown in Fig. 4a which shows that direct photolysis had no significant role in the decolorization of MB molecules. On the other hand, MB molecules were stable against the arrived photons during the irradiation process, no significant radicals were formed due to probable broking of MB bonds and about 11% of MB molecules were decolorized during 30 min of the irradiation process. Also, about 7% of MB molecules were removed by surface adsorption for 10 min and thereafter no significant increase was observed. Hence, before the decolorization experiments, all suspensions were shaken at dark for 10 min to remove the effect of the surface adsorption on MB removal. As shown, during the decolorization experiments by individual CdS and AgBr NPs and the resulted CdS-AgBr coupled system about 39%, 60%, and 80% of MB molecules were decolorized at the applied conditions, respectively. The results confirm the effectiveness of the photocatalytic decolorization process especially in the case of the coupled system. The better efficiency of the coupled system to the individual semiconductors is due to the lowest rate of e^-/h^+ recombination as confirmed by PL studies. The better role of the composite in MB photo-decolorization can be illustrated by using the typical Schematic energy diagram in Fig. 4b [56].

By focusing on this diagram, some important conclusions can be achieved. (i) Both CdS and AgBr of the coupled system can excite under the arrived photons because of their close bandgap energies. Hence, produced e^-/h^+ pairs in both semiconductors participate in the next steps for the decolorization of MB. (ii) When CdS species were excited, the produced electrons in its C_b level have a more negative E^0 value than that of the AgBr level. This favored conditions for an internal oxidation-reduction process and these photogenerated electrons could rapidly migrate to the AgBr-C_b level. In contrast, the standard potentials of their V_b levels are suitable for the whole transfer process in an opposite trend. These transference pathways for these charge carriers drastically decreased e^-/h^+ recombination and hence the coupled catalyst showed the highest degradation efficiency to the individual CdS and AgBr systems. (iii) When the moles of AgBr species were 4 times greater than that of CdS species the best photo-decolorization efficiency was observed. This confirms that in the CdS NPs electron-hole recombination was high that could limit its photocatalytic activity. When it was coupled with AgBr NPS, the mentioned phenomena in case (ii) caused to the e^-/h^+ transference and reduced e^-/h^+ recombination in CdS ingredient. Accordingly, this coupled catalyst was used for characterization techniques and in the next photo-decolorization experiments.

3.2.2. Effect of time and kinetic study of the process

Change in absorbance of MB solution during its photocatalytic decolorization is shown by the recorded UV-Vis spectra in Figs. 5a and b. Fig. 5a shows scaled spectra in the range of 400–800 nm for better clarity. Based on the literature, the UV-Vis absorption spectroscopy has confirmed that monomers and oligomers of MB are present in its aqueous solutions. The absorption peaks at 664 and 624 nm correspond to its monomer, while the absorption peaks at 606 and 565 nm correspond to its dimer and trimer, respectively

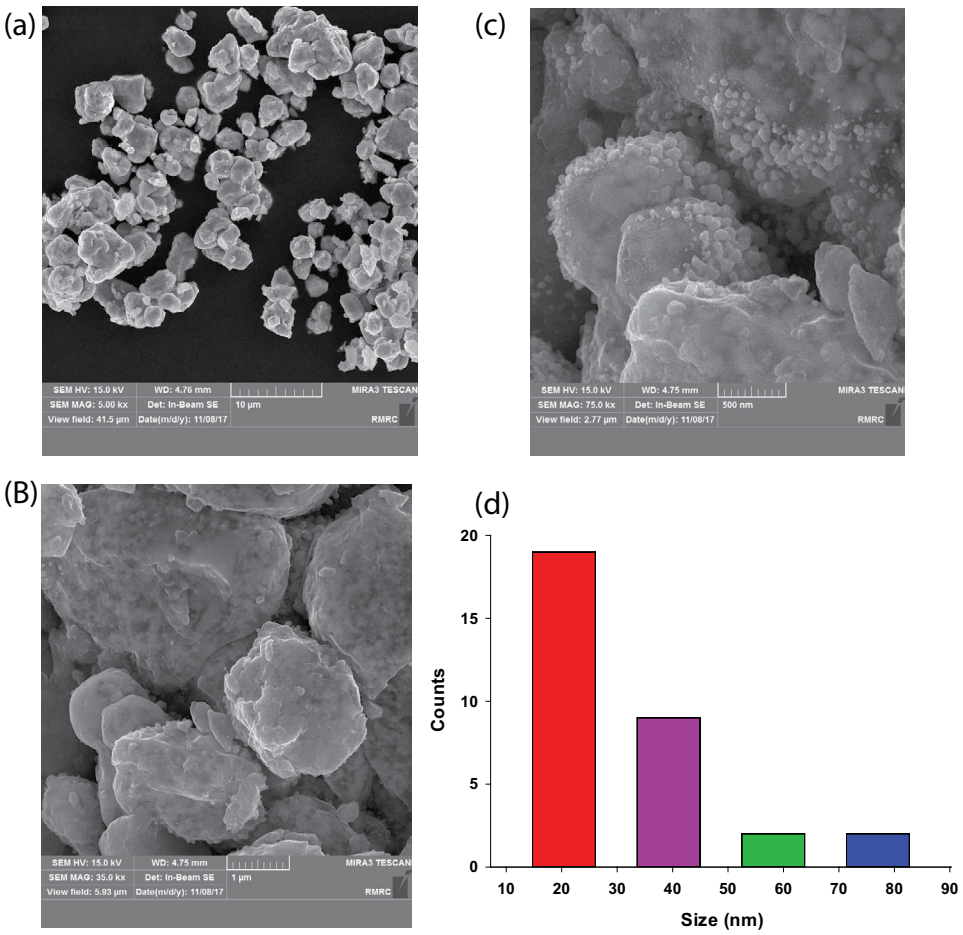

Fig. 3. Some SEM images of the coupled AgBr-CdS catalyst (a–c) and results obtained for the crystallite size distribution by applying image-j software on image c (d).

[57,58]. As shown in the spectra relative overlapping of some peaks caused to its broadening. As obvious, the most intense decrease in peak intensity was observed at the peak located at 664 nm at initial steps. This confirms that the monomers of MB molecules begun to destroy at initial times. The shoulder located at 614 nm showed a relatively slower decrease during the time. This confirms that MB dimer or trimer may be more stable than the monomer and hence they can be broken at longer times. It was reported that the molar absorptivity of MB dimer is higher than that of monomer. This may be related to the higher resonance effects in MB dimer that increases its thermodynamic stability [57]. Change in the UV-Vis spectra in the hole range of 200 to 800 nm is shown in Fig. 5b. As shown during the irradiation time, the intensity of the absorption peak at 664 nm was decreased which shows the decolorization of MB molecules. Simultaneously, the intensity of the peak at 212 nm was significantly increased which shows the degradation of MB molecules into the smaller fragments that absorb UV light photons.

The most famous model for the study of the adsorption extent of the investigated pollutants onto the catalysts surface in a heterogeneous photodegradation/decolorization process is the Langmuir-Hinshelwood (L-H) model. This model that is based on monolayer adsorption of the molecules of pollutants at the solid-liquid interface depends on the concentration of the pollutant (C). In the L-H equation (Eq. (4)), r (in mg L^{-1} min), k' (in mg L^{-1} min) and K (in L mg^{-1}) show the reaction rate, the specific reaction rate constant and the equilibrium constant, respectively [59–64].

$$r = -\frac{dC}{dt} = \frac{(k'K\,C)}{(1+K\,C)} = k'\theta \tag{4}$$

$$\ln\left(\frac{C_0}{C}\right) + k'\left(C_0 - C_t\right) = k'K\,t = k\,t \tag{5}$$

Eq. (5) shows the integrated (logarithmic) form of the L-H equation that shows an apparent first-order equation. Generally, when the initial concentration of the pollutant (C) is higher than 5 mM, Eq. (4) shows a zero-order process. In other alternatives, when the concentration is below 1 mM, an apparent first-order reaction can be adapted. During the degradation process at the time 't', the initial concentration (C_0) of the pollutant change to C_t [59–65].

The results obtained in the kinetic study of the process are shown in Fig. 5c. As shown the process well obeys from the

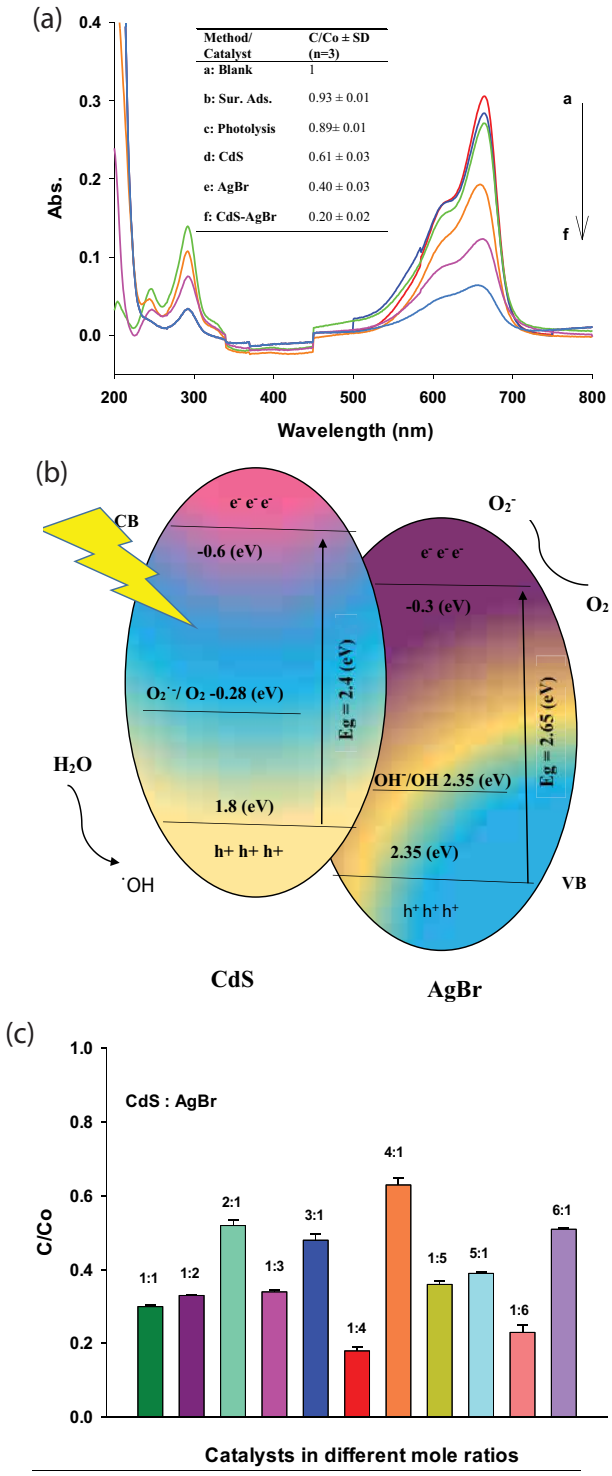

Fig. 4. (a) Change in UV-Vis spectra of MB during its removal by the mentioned removal processes: (C_{MB}: 2 ppm, amount of CdS-AgBr catalyst: 0.7 g L^{-1}, irradiation time = 30 min and initial natural pH 5.5), (b) typical energy diagram for showing charge carriers' transference in the AgBr-CdS system, and (c) change in photocatalytic activity of the AgBr-CdS coupled system by changing the mole ratio of each component (C_{MB}: 2 ppm, amount of CdS-AgBr catalyst: 0.7 g L^{-1}, pH 5.5 during 60 min).

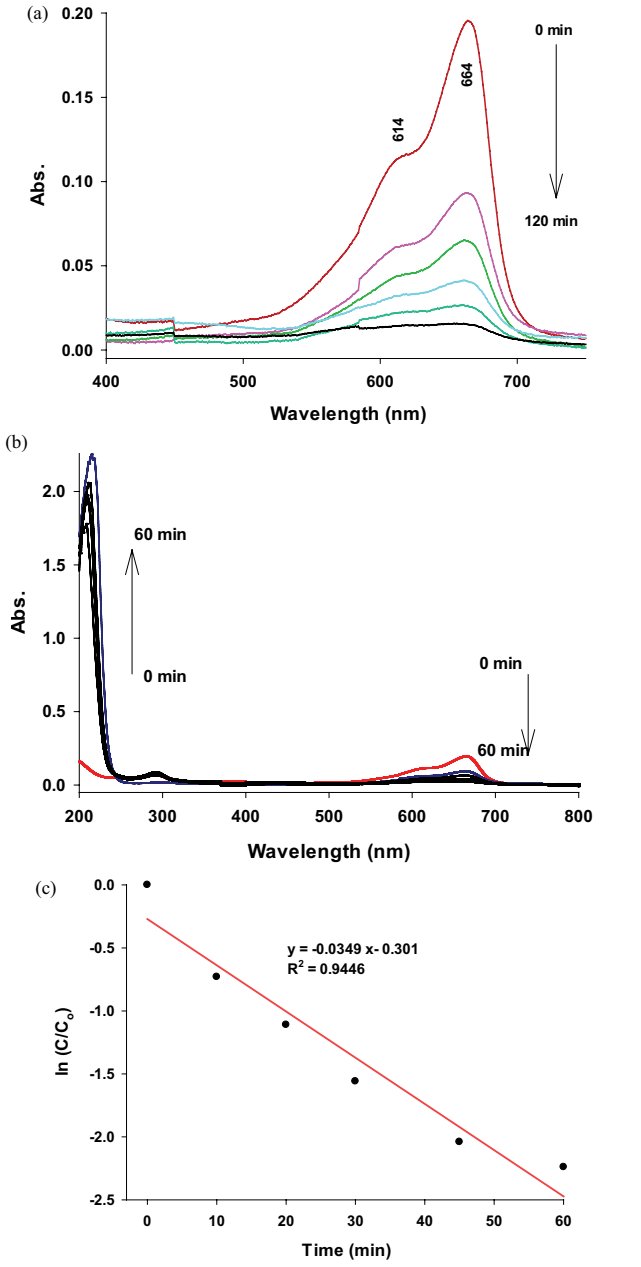

Fig. 5. (a and b) Decrease in UV–Vis absorbance for the MB solution during the irradiation process (C_{MB}: 2 ppm, amount of CdS-AgBr catalyst: 1 g L^{-1}, pH 9, irradiation time: 60 min) and (c) typical ln(C/C_0) plot vs. irradiation time for the study of kinetics of the process.

L-H model and the rate constant value of 3.49×10^{-2} min^{-1} was obtained, confirming a relatively fast photo-decolorization reaction.

3.2.3. Chemical oxygen demand and re-using studies

Mineralization of the investigated pollutant is very important because it shows decreased toxicity of the subjected water sample. The common technique used for the study of the mineralization extent of pollutants is chemical

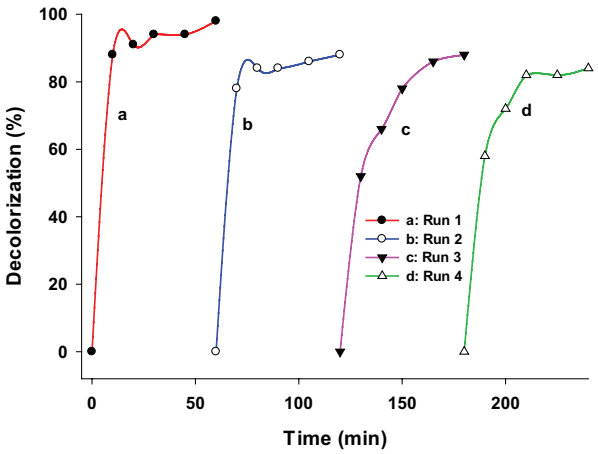

Fig. 6. Reusability in the photocatalytic activity of the coupled AgBr-CdS catalyst in photo-decolorization of MB (C_{MB} = 2 ppm, amount of catalyst = 1.0 g L^{-1}, pH 9 and irradiation time = 60 min).

oxygen demand (COD). This method is based on the required oxygen need for destroying the remained pollutants or their degradation intermediates present in the media [66]. In this work, MB solutions were subjected in the photo decolorization experiments at conditions included 2 ppm MB, 1.0 g L^{-1} of the catalyst, pH 9 at irradiation times of 30 and 60 min. The resulted solutions were subjected to COD analysis and the results were comprised of a blank solution. The COD values of 1,280; 640; and 480 mg O_2 L^{-1} were obtained for times of 0, 30 and 60 min, respectively. These values correspond to mineralization extents of 50% and 62.5% for irradiation times of 30 and 60 min, respectively. But, the decolorization extent of these solutions was about 76% and 87% as calculated by UV-Vis absorbance of the solutions. A comparison of the results confirms that the mineralization extent of MB molecules is lower than their decolorization during the mentioned irradiation times. This, in turn, confirms that some relatively stable decolorization intermediates may be formed that their mineralization needs to longer times.

Results in Fig. 6 confirm that the as-synthesized composite retained its initial activity during 4 successive re-using runs and no significant decrease in its activity was obtained. After each photo-decolorization run, the catalyst was separated by centrifugation and dried at 100°C for 10 min and used again in the next run.

4. Conclusions

The results showed an increased photocatalytic activity for the coupled AgBr-CdS catalyst to the individual AgBr and CdS semiconductors. This confirms that the presence of a high charge carriers' (e^-/h^+) separation in the composite. In this case, the photoexcited electrons in the C_b-CdS energy level can immigrate to the C_b-AgBr energy level because of the standard potential of the C_b-CdS (E^0 = –0.6 V) is more negative than that of the C_b-AgBr level (E^0 = –0.3 V). Simultaneously, the whole transfer can occur in the opposite trend, both resulting in a lower e^-/h^+ recombination process. Hence, the coupled catalyst showed higher photocatalytic activity. Decreased in e^-/h^+ recombination of the composite was confirmed by PL spectra, so the coupled catalyst had a lower PL intensity than the individual systems. When e^-/h^+ recombination diminished, the PL intensity was decreased. The mole ratio of the combined semiconductors had a vital role in the photocatalytic activity and PL intensity of the resulted composites. On the other hand, change in the mole ratio changed the rate of e^-/h^+ recombination in the coupled catalysts. Comparison of COD results and UV-Vis absorption spectroscopy results on the photo-decolorized MB molecules confirm that mineralization of MB molecules during the initial 60 min irradiation process is lower than its decolorization extent. This confirms that at initial times some decolorization intermediates may be formed that resist further mineralization and may need further time to be degraded.

References

[1] M.J. Ndolomingo, R. Meijboom, Kinetic analysis of catalytic oxidation of methylene blue over γ-Al_2O_3 supported copper nanoparticles, Appl. Catal., A, 506 (2015) 33–43.
[2] M.A. Rauf, M.A. Meetani, A. Khaleel, A. Ahmed, Photocatalytic degradation of Methylene Blue using a mixed catalyst and product analysis by LC/MS, Chem. Eng. J., 157 (2010) 373–378.
[3] A. Buthiyappan, A.R. Abdul Aziz, W.M.A. Wan Daud, Recent advances and prospects of catalytic advanced oxidation process in treating textile effluents, Rev. Chem. Eng., 32 (2015) 1–47.
[4] G. Vijayaraghavan, S. Shanthakumar, Effective removal of acid black 1 dye in textile effluent using alginate from brown algae as a coagulant, Iran. J. Chem. Chem. Eng., 37 (2018) 145–151.
[5] H. Abdolmohammad-Zadeh, E. Ghorbani, Z. Talleb, Zinc–aluminum layered double hydroxide as a nano-sorbent for removal of Reactive Yellow 84 dye from textile wastewater effluents, J. Iran. Chem. Soc., 10 (2013) 1103–1112.
[6] D. Ferhat, D. Nibou, M. Elhadj, S. Amokrane, Adsorption of Ni^{2+} ions onto NaX and NaY zeolites: equilibrium, kinetic, intra crystalline diffusion and thermodynamic studies, Iran. J. Chem. Chem. Eng., 38 (2019) 1021–9986.
[7] J. Behin, E. Ghadamnan, H. Kazemian, Recent advances in the science and technology of natural zeolites in Iran, Clay Miner., 54 (2019) 131–144.
[8] T. Hajira, A. Saud, M. Saad, Synthesis of kaolin loaded Ag and Ni nanocomposites and their applicability for the removal of malachite green oxalate dye, Iran. J. Chem. Chem. Eng., 37 (2018) 11–22.
[9] M. Bahram, S. Asadi, Gh. Karimnezhad, Synthesized poly styrene-alt-maleic acid hydrogel for removal of azo dyes, methylene blue and methyl orange, from aqueous media, J. Iran. Chem. Soc., 12 (2015) 639–645.
[10] N.M. Mahmoodi, Z. Hosseinabadi-Farahani, H. Chamani, Synthesis of nanoadsorbent and modeling of dye removal from wastewater using adaptive neuro-fuzzy inference system, Desal. Wat. Treat., 75 (2017) 245–252.
[11] A. Chaochon, S. Sirianuntapiboon, Biological textile dye removal mechanism of direct blue 15 (DB15) by anoxic/oxic-SBR system, Desal. Wat. Treat., 75 (2017) 237–244.
[12] E. Karadag, B. Yel, S. Kundakcı, Ö.B. Üzüm, Synthesis and application of acrylamide/sodium vinylsulfonate/carboxymethylcellulose/zeolite hybrid hydrogels as highly swollen effective adsorbents for model cationic dye removal, Desal. Wat. Treat., 74 (2017) 402–414.
[13] S.N. Mohseni, A.A. Amooey, H. Tashakkorian, A. Amouei, A comparative survey of linear and non-linear regression analysis on removal efficiency of clinoptilolite for sorption of dexamethasone from aqueous solutions, Desal. Wat. Treat., 67 (2017) 231–238.
[14] M.R. Gadekar, M.M. Ahammed, Coagulation/flocculation process for dye removal using water treatment residuals: modelling through artificial neural networks, Desal. Wat. Treat., 55–57 (2016) 26392–26400.

[15] T.-H. Kim, C. Park, E.-B. Shin, S.Y. Kim, Decolorization of disperse and reactive dyes by continuous electrocoagulation process, Desalination, 150 (2002) 165–175.
[16] J. Wang, L.J. Qin, J.Y. Lin, J.Y. Zhu, Y.T. Zhang, J.D. Liu, B. Van der Bruggen, Enzymatic construction of antibacterial ultrathin membranes for dyes removal, Chem. Eng. J., 323 (2017) 56–63.
[17] S.H. Lin, C.F. Peng, Continuous treatment of textile wastewater by combined coagulation, electrochemical oxidation and activated sludge, Water Res., 30 (1996) 587–592.
[18] Y.B. Zhou, J. Lu, Y. Zhou, Y.D. Liu, Recent advances for dyes removal using novel adsorbents: a review, Environ. Pollut., 252 (2019) 352–365.
[19] V. Katheresan, J. Kansedo, S.Y. Lau, Efficiency of various recent wastewater dye removal methods: a review, J. Environ. Chem. Eng., 6 (2018) 4676–4697.
[20] K. Grace Pavithra, P. Senthil Kumar, V. Jaikumar, P. Sundar Rajan, Removal of colorants from wastewater: a review on sources and treatment strategies, J. Ind. Eng. Chem., 75 (2019) 1–19.
[21] S. Krishnan, H. Rawindran, C.M. Sinnathambi, J.W. Lim, Comparison of various advanced oxidation processes used in remediation of industrial wastewater laden with recalcitrant pollutants, IOP Conf. Ser.: Mater. Sci. Eng., 206 (2017) 012089.
[22] A. Nezamzadeh-Ejhieh, M. Khorsandi, Photodecolorization of Eriochrome Black T using NiS-P zeolite as a heterogeneous catalyst, J. Hazard. Mater., 176 (2010) 629–637.
[23] Y. Deng, R. Zhao, Advanced oxidation processes (AOPs) in wastewater treatment, Curr. Pollut. Rep., 1 (2015) 167–176.
[24] B. Cuiping, G. Wenqi, F. Dexin, X. Mo, Z. Qi, C. Shaohua, G. Zhongxue, Z. Yanshui, Natural graphite tailings as heterogeneous Fenton catalyst for the decolorization of rhodamine B, Chem. Eng. J., 197 (2012) 306–313.
[25] C. EL Bekkali, H. Bouyarmane, S. Laasri, A. Laghzizil, A. Saoiabi, Effects of metal oxide catalysts on the photodegradation of antibiotics effluent, Iran. J. Catal., 8 (2018) 241–247.
[26] H. Che, G. Che, E. Jiang, C. Liu, H. Dong, C. Li, A novel Z-scheme CdS/Bi_3O_4 Cl heterostructure for photocatalytic degradation of antibiotics: mineralization activity, degradation pathways and mechanism insight, J. Taiwan Inst. Chem. Eng., 91 (2018) 224–234.
[27] K. Thirumalaia, M. Shanthia, M. Swaminathan, Natural sunlight active $GdVO_4$–ZnO nanomaterials for photo-electrocatalytic and self-cleaning applications, J. Water Process Eng., 17 (2017) 149–160.
[28] M. Karimi-Shamsabadi, M. Behpour, A. Kazemi Babaheidari, Z. Saberi, Efficiently enhancing photocatalytic activity of NiO-ZnO doped onto nanozeoliteX by synergistic effects of *p-n* heterojunction, supporting and zeolite nanoparticles in photo-degradation of Eriochrome Black T and Methyl Orange, J. Photochem. Photobiol., A, 346 (2017) 133–143.
[29] M. Shaban, M.R. Abukhadra, A. Hamd, Recycling of glass in synthesis of MCM-48 mesoporous silica as catalyst support for Ni_2O_3 photocatalyst for Congo red dye removal, Clean Technol. Environ. Policy, 20 (2018) 13–28.
[30] H. Chen, N. Chen, C. Feng, Y. Gao, Synthesis of a novel narrow-band-gap iron(II,III) oxide/titania/silver silicate nanocomposite as a highly efficient and stable visible light-driven photocatalyst, J. Colloid Interface Sci., 515 (2018) 119–128.
[31] K. Thirumalai, S. Balachandran, M. Swaminathan, Superior photocatalytic, electrocatalytic, and self-cleaning applications of Fly ash supported ZnO nanorods, Mater. Chem. Phys., 183 (2016) 191–200.
[32] S. Dianat, Visible light induced photocatalytic degradation of direct red 23 and direct brown 166 by $InVO_4$-TiO_2 nanocomposite, Iran. J. Catal., 8 (2018) 121–132.
[33] P. Raizada, J. Kumari, P. Shandilya, P. Singh, Kinetics of photocatalytic mineralization of oxytetracycline and ampicillin using activated carbon supported ZnO/$ZnWO_4$ nanocomposite in simulated wastewater, Desal. Wat. Treat., 79 (2017) 204–213.
[34] M.L. Maya-Treviño, J.L. Guzmán-Mar, L. Hinojosa-Reyes, A. Hernández-Ramírez, Synthesis and photocatalytic activity of ZnO-CuPc for methylene blue and potassium cyanide degradation, Mater. Sci. Semicond. Process., 77 (2018) 74–82.
[35] N. Masoudipour, M. Sadeghi, F. Mohammadi-Moghadam, Photo-catalytic inactivation of *E. coli* using stabilized Ag/S, N–TiO_2 nanoparticles by fixed bed photo-reactor under visible light and sunlight, Desal. Wat. Treat., 110 (2018) 109–116.
[36] N. Zhang, G. Li, T. Xie, L. Li, Amorphous tantalum oxyhydroxide homojunction: in situ construction for enhanced hydrogen production, J. Colloid Interface Sci., 525 (2018) 196–205.
[37] B.A. Ünnü, G. Gündüz, M. Dükkancı, Heterogeneous Fenton-like oxidation of crystal violet using an iron loaded ZSM-5 zeolite, Desal. Wat. Treat., 57 (2016) 11835–11849.
[38] S. Landi Jr., J. Carneiro, S. Ferdov, A.M. Fonseca, I.C. Neves, M. Ferreira, P. Parpot, O.S.G.P. Soares, M.F.R. Pereira, Photocatalytic degradation of Rhodamine B dye by cotton textile coated with SiO_2-TiO_2 and SiO_2-TiO_2-HY composites, J. Photochem. Photobiol., A, 346 (2017) 60–69.
[39] M. Salah, N. Samy, M. Fadel, Methylene blue mediated photodynamic therapy for resistant plaque psoriasis, J. Drugs Dermatol., 8 (2009) 42–49.
[40] WHO Model List of Essential Medicines (19th List) (PDF), World Health Organization, April 2015, Archived (PDF) From the Original on 13 December 2016, Retrieved 8 December 2016.
[41] Methylene Blue, The American Society of Health-System Pharmacists, Archived From the Original on 10 May 2017, Retrieved 8 January 2017.
[42] M.M. Hamed, I.M. Ahmed, S.S. Metwally, Adsorptive removal of methylene blue as organic pollutant by marble dust as eco-friendly sorbent, J. Ind. Eng. Chem., 20 (2014) 2370–2377.
[43] D. Mitoraj, U. Lamdab, W. Kangwansupamonkon, M. Pacia, W. Macyk, N. Wetchakun, R. Beranek, Revisiting the problem of using methylene blue as a model pollutant in photocatalysis: the case of $InVO_4$/$BiVO_4$ composites, J. Photochem. Photobiol., A, 366 (2018) 103–110.
[44] N. Qutub, B.M. Pirzada, K. Umar, S. Sabir, Synthesis of CdS nanoparticles using different sulfide ion precursors: formation mechanism and photocatalytic degradation of Acid Blue-29, J. Environ. Chem. Eng., 4 (2016) 808–817.
[45] D. Zhang, H. Tang, Y. Wang, K. Wu, H. Huang, G. Tang, J. Yang, Synthesis and characterization of graphene oxide modified AgBr nanocomposites with enhanced photocatalytic activity and stability under visible light, Appl. Surf. Sci., 319 (2014) 306–311.
[46] J.-Q. Xiao, K.-S. Lin, Y. Yu, Novel Ag@AgCl@AgBr hetero-structured nanotubes as high-performance visible-light photo-catalysts for decomposition of dyes, Catal. Today, 314 (2018) 10–19.
[47] B.S. Rao, B.R. Kumar, V.R. Reddy, T.S. Rao, Preparation and characterization of CdS nanoparticles by chemical co-precipitation technique, Chalcogenide Lett., 8 (2011) 177–185.
[48] P. Rodrgues, N. Muñoz-Aguirre, E. San-Martin, G. Gonzalez, Formation of CdS nanoparticles using starch as capping agent, Appl. Surf. Sci., 255 (2008) 740–742.
[49] M. Zebardast, A. Fallah Shojaei, K. Tabatabaeian, Enhanced removal of methylene blue dye by bimetallic nano-sized MOF-5s, Iran. J. Catal., 8 (2018) 297–309.
[50] P. Scherrer, Bestimmung der Grösse und der inneren Struktur von Kolloidteilchen mittels Röntgensrahlen [Determination of the size and internal structure of colloidal particles using X-rays], Nachr Ges Wiss Goettingen, Math-Phys Kl., 1918 (1918) 98-100, (In German).
[51] A. Jose, S. Devi, D. Pinheiro, S.L. Narayana, Electrochemical synthesis, photodegradation and antibacterial properties of PEG capped zinc oxide nanoparticles, J. Photochem. Photobiol., B, 187 (2018) 25–34.
[52] J. Guan, J. Li, Z. Ye, D. Wu, C. Liu, H. Wang, C. Ma, P. Huo, Y. Yan, La_2O_3 media enhance d electrons transfer for improved $CeVO_4$ @halloysite nanotubes photocatalytic activity for removing tetracycline, J. Taiwan Inst. Chem. Eng., 96 (2019) 281–298.
[53] K. Li, J. Xue, Y. Zhang, H. Wei, Y. Liu, C. Dong, $ZnWO_4$ nanorods decorated with Ag/AgBr nanoparticles as highly efficient visible-light-responsive photocatalyst for dye AR18 photodegradation, Appl. Surf. Sci., 320 (2014) 1–9.

[54] A. Nezamzadeh-Ejhieh, M. Bahrami, Investigation of the photocatalytic activity of supported ZnO–TiO_2 on clinoptilolite nanoparticles towards photodegradation of wastewater-contained phenol, Desal. Wat. Treat., 55 (2015) 1096–1104.
[55] S. Ghattavi, A. Nezamzadeh-Ejhieh, A brief study on the boosted photocatalytic activity of AgI/WO_3/ZnO in the degradation of Methylene Blue under visible light irradiation, Desal. Wat. Treat., 166 (2019) 92–104.
[56] P. Mohammadyari, A. Nezamzadeh-Ejhieh, Supporting of mixed ZnS–NiS semiconductors onto clinoptilolite nanoparticles to improve its activity in photodegradation of 2-nitrotoluene, RSC Adv., 5 (2015) 75300–75310.
[57] D. Heger, J. Jirkovsky, P. Klán, Aggregation of Methylene Blue in frozen aqueous solutions studied by absorption spectroscopy, J. Phys. Chem. A, 109 (2005) 6702–6709.
[58] S. Senobari, A. Nezamzadeh-Ejhieh, A *p-n* junction NiO–CdS nanoparticles with enhanced photocatalytic activity: a response surface methodology study, J. Mol. Liq., 257 (2018) 173–183.
[59] S. Loghambal, A.J. Agvinos Catherine, S. Velu Subash, Analysis of Langmuir-Hinshelwood kinetics model for photocatalytic degradation of aqueous direct blue 71 through analytical expression, Int. J. Math. Appl., 6 (2018) 903–913.
[60] Y. Liu, L. Shen, From Langmuir kinetics to first- and second-order rate equations for adsorption, Langmuir, 24 (2008) 11625–11630.
[61] J. Lin, L. Wang, C. Sun, Influence factors and kinetic study on photocatalytic degradation of Rhodamine B by Fe-doped TiO_2/diatomite composite, Adv. Mater. Res., 535–537 (2012) 2209–2213.
[62] G.V. Morales, E.L. Shan, R. Cornejo, E.M. Farfan Torres, Kinetic studies of the photocatalytic degradation of tartrazine, Lat. Am. Appl. Res., 42 (2012) 45–49.
[63] A. Nezamzadeh-Ejhieh, Z. Ghanbari-Mobarakehi, Heterogeneous Photodegradation of 2,4-dichlorophenol using FeO doped onto nanoparticles of zeolite P, J. Ind. Eng. Chem., 21 (2015) 668–676.
[64] N. Omrani, A. Nezamzadeh-Ejhieh, M. Alizadeh, Brief study on the kinetic aspect of photodegradation of sulfasalazine aqueous solution by cuprous oxide/cadmium sulfde nanoparticles, Desal. Wat. Treat., 162 (2019) 290–302.
[65] M. Zarifeh-Alsadat, A. Nezamzadeh-Ejhieh, Removal of phenol content of an industrial wastewater via a heterogeneous photodegradation process using supported FeO onto nanoparticles of Iranian clinoptilolite, Desal. Wat. Treat., 57 (2016) 16483–16494.
[66] S.A.P. Pereira, S.P.F. Costa, E. Cunha, M.L.C. Passos, A.R.S.T. Araújo, M.L.M.F.S. Saraiva, Manual or automated measuring of antipsychotics' chemical oxygen demand, Ecotoxicol. Environ. Saf., 152 (2018) 55–60.

Supplementary information

Table S1
Data used in Scherrer equation for the estimation of crystallite size of CdS-AgBr composite

2θ (°)	θ (°)	θ (rad)	Cos θ (rad)	β (rad)	d (nm)	$\bar{d} \pm SD$
26.973	13.487	0.234	1	0.00394	35.02	
31.187	15.594	0.271	1	0.00403	34.07	
44.567	22.284	0.387	1	0.00487	28.39	29.03 ± 5.4
52.752	26.376	0.458	1	0.00567	24.38	
55.260	27.630	0.480	1	0.00594	23.27	